PUBLICATIONS OF THE ASTRONOMICAL SOCIETY OF THE PACIFIC, **117**:1263–1270, 2005 November

Establishing Visible Interferometer System Responses: Resolved and Unresolved Calibrators

GERARD T. VAN BELLE

Michelson Science Center, California Institute of Technology, Pasadena, CA 91125; gerard@ipac.caltech.edu

AND

GERALD VAN BELLE

Department of Biostatistics, University of Washington, Seattle, WA 98195-7232; vanbelle@seanet.com

Received 2005 May 12; accepted 2005 July 8; published 2005 September 28

ABSTRACT. This investigation examines the propagation of errors through the uniform disk visibility function. The implications of those errors on measurements of absolute visibility through optical and near-infrared interferometers are considered within the context of using calibration stars to establish system visibilities for these instruments. We suggest a simple ratio test to establish empirically whether or not the measured visibilities produced by such an instrument are relative (errors dominated by calibrator angular size prediction error) or absolute (errors dominated by measurement error).

Online material: color figures

1. INTRODUCTION

Visible and near-infrared interferometers are powerful tools for measuring the minute angular sizes of nearby stars. However, establishing absolute system responses in the presence of atmospheric turbulence and instrument imperfections is a challenging proposition that requires careful attention to detail when constructing an observational approach.

For two-element interferometers that are now commonly in use, the principal measured quantity is the visibility V, which is simply a characterization of the contrast found in the observed interference fringe, and can range from 0 to 1. In practice, interferometers that lock onto and track fringes through temporally modulating servo loops tend to measure V^2 rather than just V. A detailed discussion of fringe-visibility estimators can be found in Colavita (1999).

For individual stars, the observed V^2 will decrease from unity as the source becomes resolved to the instrument, and also as the response of the instrument and atmosphere through which it observes departs from an idealized system. A common approach to account for the system response (a combination of the atmospheric and instrumental responses) is to interleave observations of calibration stars with observations of the star of interest. If the system visibility $V^2_{\rm sys}$ is established with calibration sources, a target star's absolute V^2 is then easily derived from the measured V^2:

$$V^2_{\rm norm}({\rm target}) = \frac{V^2_{\rm meas}({\rm target})}{V^2_{\rm sys}}. \qquad (1)$$

Calibration sources are stars for which we have some sort of a priori knowledge of their angular size, and as a result, their expected values for V^2 can be predicted ($V^2_{\rm pred}$). Thus, from the calibrator's measured V^2 values ($V^2_{\rm meas}$), the system visibility $V^2_{\rm sys}$ that characterizes the atmospheric and instrumental performance degradations is simply

$$V^2_{\rm sys} = \frac{V^2_{\rm meas}({\rm calibrator})}{V^2_{\rm pred}({\rm calibrator})}. \qquad (2)$$

It is important to note that, as is apparent from the practice of using the system visibility found in equations (1) and (2), the system visibility needs to be constant when observing both the target star and the calibration star. This consideration is significant when such objects are of differing brightness, are located in different portions of the sky, are subject to varying weather conditions, or are widely separated in time. Because no two stars will be of exactly the same brightness, the instrument will be required to have some measure of dynamic range in this regard; for the purposes of this investigation, we assume all of the relevant data are properly collected within the range of constant system visibility.

For some of the sources considered for use as calibrators, angular sizes have actually been measured. However, for most of the sources considered as calibrators, some sort of indirect estimation technique needs to be employed. These techniques include angular size estimation from distance and linear size (with the second quantity often being inferred from some proxy, such as spectral type), blackbody fitting, $R - I$ and $V - K$ proxies (Mozurkewich et al. 1991; di Benedetto 1993; van Belle

1999), and spectrophotometric fits (Blackwell & Lynas-Gray 1994; Cohen et al. 1996).

For unbiased results, it is preferable to utilize calibration sources that are "unresolved" to the interferometer. A source is considered to be unresolved when the errors in $V^2_{\rm sys}$ are dominated by the measurement error and not the prediction error $[(\sigma_{V^2})_{\rm meas} > (\sigma_{V^2})_{\rm pred}]$. For such a calibrator, biases in the angular size estimation technique—known or unknown—are masked by the measurement process. This is due the interferometer's insensitivity to the unresolved calibrator's angular size, and as such, this technique is insensitive to estimation technique biases. In the limit that the instrument performance is linear between target and calibration sources, the resulting calibration is thus considered to be an *absolute calibration* of the system visibility $V^2_{\rm sys}$. This approach is documented in the literature for many interferometers, including the Mark III (Mozurkewich et al. 1991), the Infrared Michelson Array (IRMA; Dyck et al. 1993), the Infrared Optical Telescope Array (IOTA; Dyck et al. 1996), and the Palomar Testbed Interferometer (PTI; van Belle et al. 1999). In addition, as we see in § 3, this approach avoids the regime in which the separate Taylor series bias due to nonlinearity in the error propagation technique becomes significant as well.

Another approach seen with some regularity is the establishment of system $V^2_{\rm sys}$ through use of resolved calibrators. In the case where instrumental limitations (typically limited sensitivity) preclude the use of an unresolved calibrator, investigators have utilized calibration sources that are resolved to establish instrument system visibilities. The strength of this approach is that resolved calibrators are typically associated with stars of greater brightness, and as a result, a greater signal-to-noise ratio (S/N) is achieved in observing the calibration sources.

The weakness of this approach is that it establishes only a *relative calibration* for the measurement, and any biases inherent in the original size estimation of the calibration source propagate into the final visibility measured for the target source, albeit with additional uncertainty due to measurement error in $V^2_{\rm meas}$. Relative V^2 measurements, when properly used, are useful quantities for certain investigations—for example, in the examination of the shape of a rotationally distorted star (Domiciano de Souza et al. 2003)—but are inappropriate to use as absolute values to establish quantities such as stellar linear size or effective temperature.

2. THE VISIBILITY FUNCTION AND ANGULAR SIZE ESTIMATION BIAS

The projections of stellar disks on the sky are clearly not true "uniform disks" (see Hajian et al. 1998 and references therein), having varying brightness from the center to the edge of their disks. However, for most stars, characterization of them as uniform disks is a reasonable approximation, and one that lends itself to a mathematical examination in § 2.1.

A uniform disk as viewed by an interferometer exhibits a visibility function w, given by

$$V(x)^2 = w(x) = \left[\frac{2J_1(x)}{x}\right]^2 = \left[\frac{2J_1(\pi\theta B/\lambda)}{\pi\theta B/\lambda}\right]^2, \qquad (3)$$

where x is the spatial frequency and is a function of projected baseline B, source angular size θ, and observational wavelength λ (Airy 1835; Born & Wolf 1980).

Since we will be utilizing calibration sources with predicted angular sizes θ, it is of great utility to examine the impact that errors (and potentially size-estimation biases) have on our expected values for calibration source $V^2_{\rm pred}$.

2.1. Uniform Disk Visibility Error Propagation

Since $w = w(\theta, B, \lambda)$, a routine propagation of errors through equation (3) gives

$$\sigma_w^2 = \left(\frac{\partial w}{\partial \theta}\right)^2 \sigma_\theta^2 + \left(\frac{\partial w}{\partial B}\right)^2 \sigma_B^2 + \left(\frac{\partial w}{\partial \lambda}\right)^2 \sigma_\lambda^2 + \mathrm{cov}(\theta, B, \lambda), \qquad (4)$$

for which the covariance terms for this discussion are expected to be zero (we reexamine the higher order terms of eq. [4] in § 3). For the evaluation of equation (4), it is useful to employ the jinc(x) function, which is defined in Bracewell (2000), and its first derivative, given as

$$\mathrm{jinc}\,(x) = \frac{J_1(x)}{x} \quad \text{and} \quad \mathrm{jinc}'\,(x) = -\frac{J_2(x)}{x}. \qquad (5)$$

Using the chain rule on equations (3) and (4),

$$\begin{aligned}\frac{\partial w}{\partial x} &= \frac{\partial}{\partial x}\left[\left(\frac{2J_1(x)}{x}\right)^2\right] \\ &= \frac{\partial}{\partial x} 4\,\mathrm{jinc}\,(x)^2 \\ &= 8\,\mathrm{jinc}\,(x)\,\mathrm{jinc}'\,(x) \\ &= -\frac{8J_1(x)J_2(x)}{x^2}. \end{aligned} \qquad (6)$$

Equation (4) can be rewritten as

$$\begin{aligned}\sigma_w^2 &= \left[-\frac{8J_1(x)J_2(x)}{x^2}\right]^2 \left[\left(\frac{\pi B}{\lambda}\right)^2 \sigma_\theta^2 + \left(\frac{\pi\theta}{\lambda}\right)^2 \sigma_B^2 + \left(-\frac{\pi B\theta}{\lambda^2}\right)^2 \sigma_\lambda^2\right] \\ &= \left[\frac{8J_1(x)J_2(x)}{x}\right]^2 \left[\left(\frac{\sigma_\theta}{\theta}\right)^2 + \left(\frac{\sigma_B}{B}\right)^2 + \left(\frac{\sigma_\lambda}{\lambda}\right)^2\right]. \end{aligned} \qquad (7)$$

In the limit that the calibrator size prediction fractional errors

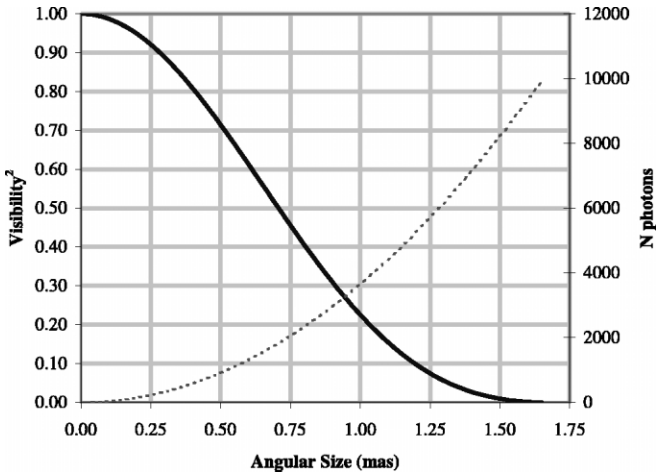

FIG. 1.—Visibility V^2 for uniform disk stars as viewed by the CHARA Array, with a 330 m baseline and a K_s bandpass. Also shown on the right vertical axis with a gray dotted line is detected photon count N, assuming a G2 V calibration source, a 0.001 ms integration time per sample, 1 m diameter aperture, and 4% throughput. [*See the electronic edition of PASP for a color version of this figure.*]

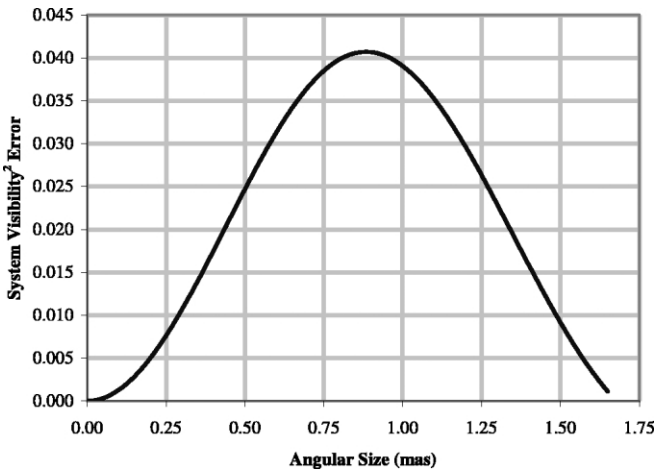

FIG. 2.—Calibrator V^2 prediction error $(\sigma_{V^2})_{\rm pred}$ propagated from an assumed 5% uncertainty in calibrator angular size, *not* accounting for measurement error. [*See the electronic edition of PASP for a color version of this figure.*]

dominate ($\sigma_\theta/\theta \gg \sigma_B/B, \sigma_\lambda/\lambda$), we have

$$(\sigma_{V^2})_{\rm pred} = \sigma_w = \left[\frac{8J_1(x)J_2(x)}{x}\right]\left(\frac{\sigma_\theta}{\theta}\right). \quad (8)$$

This error propagates in quadrature back to our estimate of the system visibility in equation (2), along with any measurement error $(\sigma_{V^2})_{\rm meas}$.

In considering $(\sigma_{V^2})_{\rm meas}$, it is very important not only to establish the measurement scatter of a single V^2 sampling event, but to empirically establish the night-to-night measurement error found in V^2 measurements. An excellent example of such a characterization is the examination of the final V^2 residuals in the binary-star fit of ι Pegasi found in Boden et al. (1999).

2.2. Absolute versus Relative Ratio Test

We can use equations (7) and (8) to explore the impact that calibrator size prediction error has σ_θ on the system visibility error $(\sigma_{V^2})_{\rm pred}$. Our test case is as follows: a 330 m baseline with a $\sigma_B = 1$ cm error in its knowledge of projection on the sky (which will be the product of geometry knowledge errors and timing errors, but is still a generous error bar for this term); a $\sigma_\lambda = 0.01$ μm error in the knowledge of the operational wavelength ($\lambda = 2.15$ μm); and a 5% prediction error σ_θ in the angular size estimate for an individual calibrator. This test case is fairly representative of the current parameters of interest for the CHARA Array (ten Brummelaar et al. 2005).

For a range of angular sizes, the predicted V^2 value for the calibrator is plotted in Figure 1. As the star passes 0.690 mas, V^2 has already fallen below 50% and drops to zero beyond 1.500 mas. Also plotted in Figure 1 on the righthand axis is a rough expectation of the number of detected photons N for the CHARA Array for a G2 V star, following the relationship detailed in van Belle (1999) between $V - K$ and angular size (noting that the estimate of system throughput may be inaccurate but only scales the results here). For our hypothetical G2 V star, we have $V - K = 1.5$ (Bessell & Brett 1988). The predicted V^2 error derived from those values for the three error terms in equation (7) is shown in Figure 2. We can also estimate our S/N as being proportional to N^2V^2 in the read-noise–limited regime (the usual operational case for near-infrared interferometers; Colavita 1999), although we note that a similar analysis we have executed for NV^2 gives results similar to those presented in this section and the next. (This latter case corresponds to photon-noise–limited operations [Mozurkewich et al. 1991] in the low-photon limit, as might be the case for visible interferometers.) A plot of this is shown in Figure 3, which is effectively the product of the solid line and the dotted line squared seen in Figure 1.

One way to illustrate this point is to examine the ratio r of V^2 measurement error $(\sigma_{V^2})_{\rm meas}$ to calibrator V^2 prediction error $(\sigma_{V^2})_{\rm pred}$, as is seen in Figure 4:

$$r = \frac{(\sigma_{V^2})_{\rm meas}}{(\sigma_{V^2})_{\rm pred}}. \quad (9)$$

The range of angular sizes at which r dips below 1.0 indicates where $(\sigma_{V^2})_{\rm pred}$ is a significant, if not the dominant, contribution to the V^2 measurement error. Equation (9) (with the denominator as provided by eq. [7] or [8]) is a straightforward indicator of the interferometer operational regime as determined by the

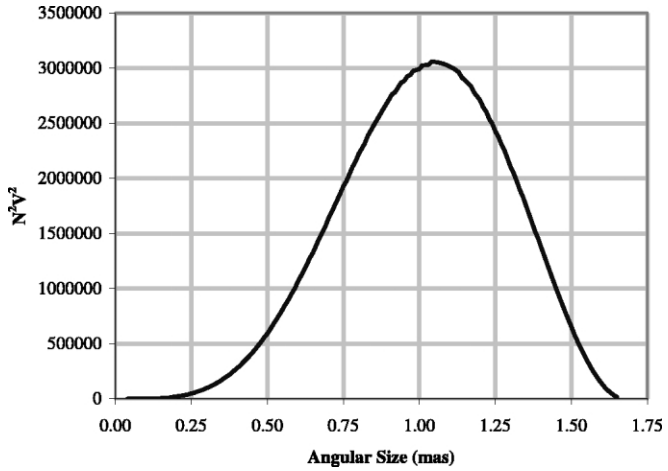

FIG. 3.—S/N (N^2V^2) for our G2 V source as a function of calibrator angular size. [*See the electronic edition of PASP for a color version of this figure.*]

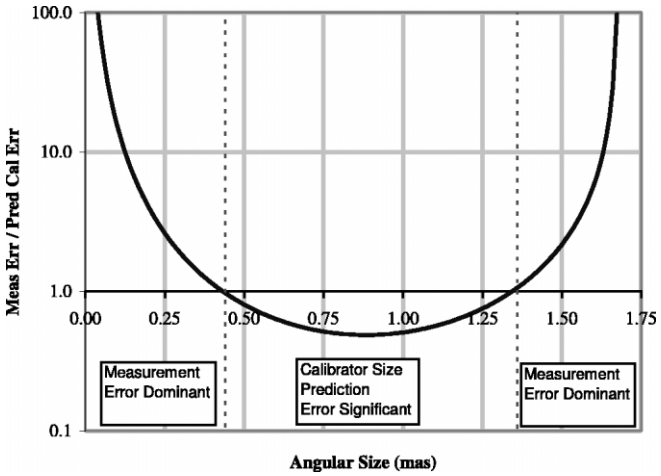

FIG. 4.—From eq. (9), the ratio of an assumed 2% V^2 measurement error to the V^2 error due to calibrator size prediction error of 5%, as a function of expected calibrator size. Note the regime between the gray dotted lines ($0.45 < \theta < 1.35$ mas), where the $(\sigma_{V^2})_{\rm pred}$ has a significant impact on the final errors. [*See the electronic edition of PASP for a color version of this figure.*]

choice of calibrator: for $r < 1$ it is relative, and for $r > 1$ it is absolute.

It is interesting to note that Figure 4 indicates a second regime of absolute calibrator sizes for our example case; that of the "superresolved" sources in the range of $\theta > 1.35$ mas. Simply put, it is in this regime that the V^2 function has once again flattened out (see Fig. 1), and uncertainty in θ does little to impact $V^2_{\rm pred}$ for the calibrator. Unfortunately, it is also in this range that the S/N rapidly drops to zero, as already seen in Figure 3. In addition, as we see in § 3, this regime is problematic due to bias in the error propagation technique.

2.3. A Merit Function and its Evaluation

As a useful metric of "calibrator goodness," we propose a merit function equal to the ratio of S/N to system visibility error:

$$m = \frac{N^2V^2}{\sigma_{V^2}}. \tag{10}$$

In the real-world case, V^2 measurement error $(\sigma_{V^2})_{\rm meas}$ also affects our measurements of the system visibility. The resulting system visibility error is computed from the measurement error and the calibrator V^2 prediction error, added in quadrature,

$$\sigma^2_{V^2} = (\sigma_{V^2})^2_{\rm meas} + (\sigma_{V^2})^2_{\rm pred}, \tag{11}$$

and applied to our merit function. The merit function incorporating the measurement error and calibrator size prediction error is plotted in Figure 5 for the case in which the V^2 measurement errors are assumed to be at the 2% level.

Of interest in our CHARA Array example are the angular sizes beyond ~0.450 mas, where the merit function changes slope, peaks, and descends. It is at those angular sizes ($\theta > 0.450$ mas) that the contribution to the merit function transitions from V^2 measurement error $(\sigma_{V^2})_{\rm meas}$ being dominant to calibrator V^2 prediction error $(\sigma_{V^2})_{\rm pred}$ becoming significant and then dominant. This regime is of particular interest: if the technique being employed for calibrator V^2 prediction is subject to a systematic size-estimation bias due to an imperfection in the predictive technique, that bias will begin to significantly affect the inferred V^2 values for calibrators in excess of the

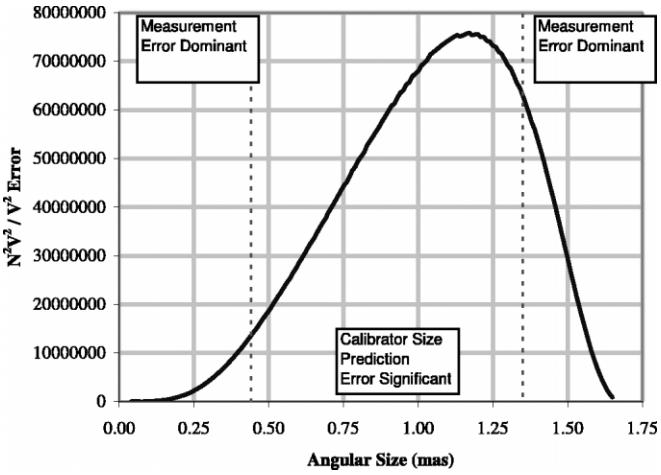

FIG. 5.—Full calibrator merit function N^2V^2/σ_{V^2}, propagated from an assumed 5% uncertainty in calibrator angular size, and including a putative 2% V^2 measurement error. The regime to the left of the gray dotted line (in the case of this example, $0 < \theta < 0.45$ mas) has measurement error as the dominant contribution to the merit function. [*See the electronic edition of PASP for a color version of this figure.*]

size, despite their apparent greater "merit" indicated by equation (10). For calibrators short of this point, any systematic size-estimation biases in the size prediction (and resulting V^2 prediction) will be masked by the calibrator's pointlike nature for the interferometer system.

2.4. Stellar Angular Size Prediction Bias Example: The Blackbody Case

If we consider stars as blackbodies (as is frequently done), we can fit broad- and narrowband photometry from these objects using a Planck function, which will result in predictions for the object's effective temperature, bolometric flux, and angular size. However, such an approximation is quite poor and overlooks many subtleties of stellar atmospheres, such as wavelength-dependent opacities.

In order to quantify the specifics of this example, a sample of 48 late giant stars from van Belle et al. (1999) that were well characterized photometrically was examined with such an approximation. The benefit of this sample is that the sizes are measured and presented in van Belle et al. (1999) and can be compared to the results obtained with the blackbody fit. Figure 6 plots the ratio of measured angular size to blackbody-derived angular size, as a function of the effective temperatures established for those stars in the paper. Errors in the blackbody angular size were derived from appropriate iteration of the Planck function within the errors specified for the photometry.

What is interesting to note in Figure 6 is the systematic offset of the ratios below a line of unity—the blackbody technique systematically delivers an angular size that is too large relative to the sizes that have been measured. The errors in that ratio, propagated from the blackbody and measured angular size errors, indicate that the ratio of unity is within most of the displayed error bars, as one would expect, but the general trend (on the order of ~15%–25%) shows that use of simple blackbody angular sizes could potentially bias interferometer calibrators.

As an example, if we were to use these sorts of stars in this manner with the PTI, we would find that for *K*-band operations with its 110 m baseline, we would need stars in the $\theta \leq 0.45$–58 mas range for use as absolute calibrators, given the PTI's limiting measurement precision of $(\sigma_{V^2})_{\rm meas} = 0.014$ (Boden et al. 1999) used in equations (8) and (9), with a requirement of $r > 1$. With this approach, our previous CHARA Array example with $(\sigma_{V^2})_{\rm meas} = 0.020$ would require $\theta \leq 0.20$ mas, which would demand distant calibration objects beyond its sensitivity limits. Fortunately, techniques have been developed with the apparent ability to predict stellar angular sizes to better than 10%, such as spectral energy distribution fitting (e.g., Blackwell & Lynas-Gray [1994] and Cohen et al. [1999] agree with interferometric measurements at the ~few percent level), allowing for the use of very long baseline instruments, such as the CHARA Array, in an absolute fashion.

Clearly, more sophisticated approaches to angular size estimation can be undertaken for interferometer calibrator stars, presumably with less susceptibility to size-estimation bias, but the blackbody example is illustrative of how it demonstrates potential bias within an estimation technique. One of the most useful aspects of an astronomical interferometer, however, is its ability to mask bias in a calibrator size prediction technique for a sufficiently unresolved calibration source, and in doing so, deliver absolutely calibrated visibilities. Such an approach is not merely useful, but is essential to calibrate and verify predictive techniques of ever-increasing accuracy.

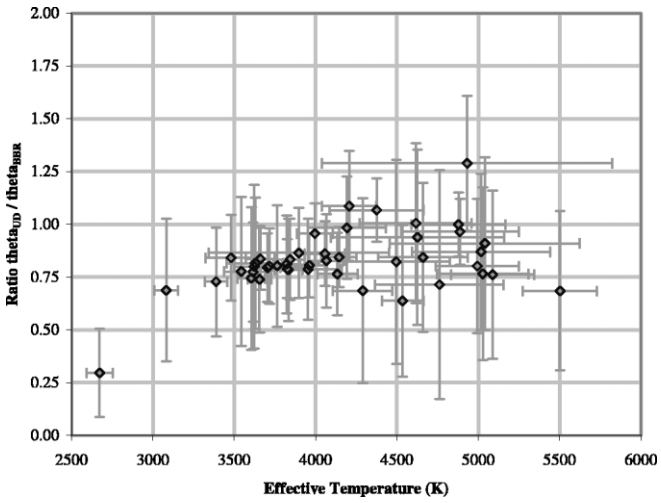

FIG. 6.—Ratio of measured angular size to predicted angular size (as derived from a blackbody approximation) as a function of effective temperature for 48 stars from van Belle et al. (1999). [*See the electronic edition of PASP for a color version of this figure.*]

3. TAYLOR SERIES BIAS IN THE ERROR PROPAGATION TECHNIQUE

The "routine propagation of errors" given in equation (4) is based on just the first term of the Taylor series, which is subject to inaccuracies as the equation becomes more nonlinear. This particular approximation is increasingly inaccurate for nonlinear equations. Expanding on our discussion of error propagation in § 2.1 to probe the significance of the higher order terms, we can expand equation (3) in a Taylor series about a given spatial frequency μ:

$$w(x|\mu) = w(\mu|\mu) + (x-\mu)w'(\mu|\mu) + \frac{(x-\mu)^2}{2!}w''(\mu|\mu) + \dots . \quad (12)$$

The average of $w(x|\mu)$ can be written as

$$\overline{w(x|\mu)} = w(\mu|\mu) + \frac{\sigma_x^2}{2!}w''(\mu|\mu) + \dots , \quad (13)$$

since to first order, the $(x - \mu)w'(\mu|\mu)$ term drops out if x is centered around the mean μ. The usual error propagation presented in equation (4) assumes that the last term in equation (13) is also negligible, which represents the Taylor series bias in the error propagation method:

$$\text{bias}_T = \overline{w(x|\mu)} - w(\mu|\mu) = \frac{\sigma_x^2}{2!} w''(\mu|\mu). \quad (14)$$

From equations (3), (5), and (8), we can write this as

$$\text{bias}_T = \frac{\sigma_x^2}{2!} \{8[\,\text{jinc}'(\mu)]^2 - 8\,\text{jinc}(\mu)\,\text{jinc}''(\mu)\}\,. \quad (15)$$

Both jinc and jinc′ are found in equation (5), and a derivation of jinc″ can be found in the Appendix.

For most applications (including the examples given here), σ_x is dominated by the uncertainty in predicted calibrator angular size, $(\sigma_\theta)_{\text{pred}}$. As such, our example of 5% error in θ means $\sigma_x = 5\% \times x$; the percentage bias as a function of calibrator predicted visibility $[\text{bias}_T(\mu)/V(\mu)^2]$ is plotted in Figure 7 for our CHARA Array test case. The bias_T term in this case starts to grow exponentially at $\theta \gtrsim 1.25$ mas; because of this, the "superresolved" calibrator regime indicated in Figure 4 and discussed in § 2.3 is undesirable for use as a source of calibrators.

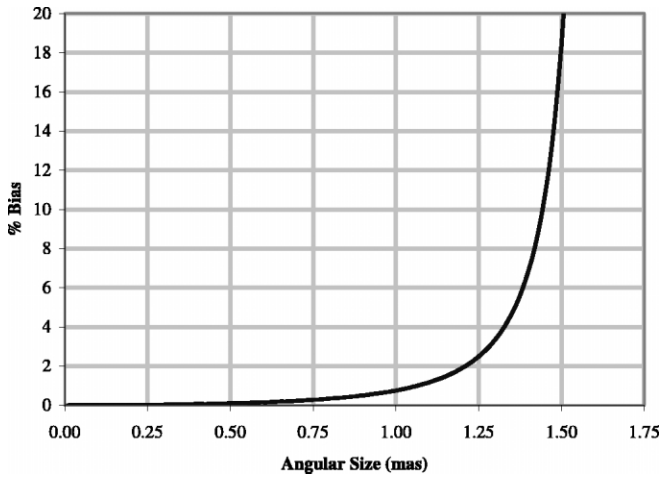

FIG. 7.—Percentage of Taylor series bias in a V^2 measurement, as discussed in § 3, due to calibrator size prediction error of 5%, as a function of expected calibrator size. [*See the electronic edition of PASP for a color version of this figure.*]

4. DISCUSSION

Predictive techniques are clearly imperfect—otherwise, why would we bother with measuring stellar angular sizes through V^2 measurements in the first place? As such, it is essential that work be carried out in the regime that is unaffected by potential bias in the calibrator angular size predictive technique, or bias from nonlinearities in the visibility function.

Permutations on the sample CHARA Array case in § 2.2 are worth considering. While a 5% angular size prediction error is reasonable to expect for most calibration sources, for those sources with the very best a priori spectrophotometric characterization, a 2.5% prediction error may be possible. In this case, a 0.5% error in the knowledge of operational wavelength ($\sigma_\lambda = 0.01$ μm for K_s in eq. [7]) still only contributes to the V^2 prediction error value by a factor of approximately ~1.02; prior angular size knowledge at the <1% level is necessary for this error term to contribute at a level greater than ~1.10.

As the measurement precision increases [and $(\sigma_{V^2})_{\text{meas}}$ decreases], the unity crossing point seen in Figure 4 (where one passes from the absolute measurement regime into the relative measurement regime) decreases in value, ranging from ~0.62 mas in the case of 5% errors (typically associated with nonspatially filtered systems) down to ~0.40 mas for 1.5% errors (typical of systems with spatial filtering). This is rather intuitive: as one's interferometric instrumentation improves in its ability to precisely measure visibilities, the degree to which that instrumentation is sensitive to potential biases in calibrator visibility prediction increases.

These values scale with spatial frequency, which will itself scale linearly with wavelength and baseline length for individual facilities. A selection of currently operational facilities is cited in Table 1, along with their relevant operational parameters of operational baseline, wavelength, and cited measurement precision. From these values, the maximum calibrator angular size for absolute angular size measurements is derived using the process found in § 2.3, assuming a 5% angular size estimation error.

5. CONCLUSION

Given the common use of optical and near-infrared interferometers to establish basic stellar parameters such as linear radius and effective temperature, it is of paramount importance to clearly understand the operational regime of one's instrument as defined not only by its intrinsic capabilities, but also by the particulars of the observing technique. As shown in § 2, in the case in which resolved calibrators are employed, the interferometric visibility measurements that are provided are relative, and as such are subject to biases—known and unknown—in the calibrator diameter estimation process employed.

The use of unresolved calibrators found in the regime as defined by the ratio test of equation (9) is *essential* to making absolute measurements. Additionally, as seen in § 3, the nonlinear nature of the visibility function makes the routine propagation of errors incorrect for very low visibilities, and as such, biases the V^2 measurements as well.

TABLE 1
MAXIMUM CALIBRATOR SIZES

Facility	Maximum Baseline (m)	Band	Cited V^2 Measurement Error	Maximum Calibrator Size (mas)	Notes	Reference
CHARA	330	*K*	0.04	0.77	No spatial filtering	van Belle et al. (2005)
	330	*K*	0.02	0.45	Spatial filtering	Under development
IOTA	38	*J*	0.046	2.3	No spatial filtering	Millan-Gabet et al. (2005)
NPOI	37.5	*V*	0.02	1.0	No spatial filtering	Tycner et al. (2004)
PTI	110	*K*	0.014	1.1	Spatial filtering	Boden et al. (1999)
VLTI	187	*K*	0.004	0.31	Spatial filtering, photometric monitoring	Kervella et al. (2003)

NOTE.—Maximum calibrator sizes for absolute calibration of V^2 measurements for a variety of current interferometric facilities, assuming 5% calibrator size estimate errors.

We would like to thank Theo ten Brummelaar and Andy Boden for proofreading and offering thoughtful suggestions. This manuscript significantly benefited from the comments of an anonymous referee. Portions of this work were performed at the California Institute of Technology, under contract with the National Aeronautics and Space Administration.

APPENDIX A

DERIVATION OF jinc″(*x*)

Starting with the two Bessel function identities

$$\frac{d}{dx}\left[x^m J_m(x)\right] = x^m J_{m-1}(x) \tag{A1}$$

and

$$J_{-m}(x) = (-1)^m J_m(x), \tag{A2}$$

we can use the recurrence relation

$$J_\nu(z) = \frac{2(\nu-1)}{z} J_{\nu-1}(z) - J_{\nu-2}(z) \tag{A3}$$

as applied to J_2,

$$J_2(z) = \frac{2}{z} J_1(z) - J_0(z), \tag{A4}$$

and explicitly work out jinc″(*x*):

$$\begin{aligned}
\mathrm{jinc}''(x) &= \frac{d}{dx}\,\mathrm{jinc}'(x) \\
&= \frac{d}{dx}\left[\frac{-J_2(x)}{x}\right] \\
&= \frac{d}{dx}\left\{\frac{1}{x}\left[J_0(x) - \frac{2}{x}J_1(x)\right]\right\} \\
&= \left\{\frac{-1}{x^2}\left[J_0(x) - \frac{2}{x}J_1(x)\right]\right\} + \left\{\frac{1}{x}\left[-J_1(x) + \frac{2}{x}J_2(x)\right]\right\}.
\end{aligned} \tag{A5}$$

REFERENCES

Airy, G. B. 1835, Trans. Camb. Philos. Soc., 5, 283
Bessell, M. S., & Brett, J. M. 1988, PASP, 100, 1134
Blackwell, D. E., & Lynas-Gray, A. E. 1994, A&A, 282, 899
Boden, A. F., et al. 1999, ApJ, 515, 356
Born, M., & Wolf, E. 1980, Principles of Optics (6th ed.; Oxford: Pergamon Press)
Bracewell, R. N. 2000, The Fourier Transform and its Applications, ed. R. N. Bracewell (Boston: McGraw Hill)
Cohen, M., Walker, R. G., Carter, B., Hammersley, P., Kidger, M., & Noguchi, K. 1999, AJ, 117, 1864
Cohen, M., Witteborn, F. C., Carbon, D. F., Davies, J. K., Wooden, D. H., & Bregman, J. D. 1996, AJ, 112, 2274
Colavita, M. M. 1999, PASP, 111, 111
di Benedetto, G. P. 1993, A&A, 270, 315
Domiciano de Souza, A., Kervella, P., Jankov, S., Abe, L., Vakili, F., di Folco, E., & Paresce, F. 2003, A&A, 407, L47
Dyck, H. M., Benson, J. A., & Ridgway, S. T. 1993, PASP, 105, 610
Dyck, H. M., Benson, J. A., van Belle, G. T., & Ridgway, S. T. 1996, AJ, 111, 1705

Hajian, A. R., et al. 1998, ApJ, 496, 484
Kervella, P., Thévenin, F., Ségransan, D., Berthomieu, G., Lopez, B., Morel, P., & Provost, J. 2003, A&A, 404, 1087
Millan-Gabet, R., Pedretti, E., Monnier, J. D., Schloerb, F. P., Traub, W. A., Carleton, N. P., Lacasse, M. G., & Segransan, D. 2005, ApJ, 620, 961
Mozurkewich, D., et al. 1991, AJ, 101, 2207
ten Brummelaar, T., et al. 2005, ApJ, 628, 453
Tycner, C., et al. 2004, AJ, 127, 1194
van Belle, G. T. 1999, PASP, 111, 1515
van Belle, G. T., et al. 1999, AJ, 117, 521
———. 2005, ApJ, in press